One- and two-color laser spectroscopy of indium vapor in an all-sapphire cell

U. Rasbach, J. Wang, R. dela Torre, V. Leung, B. Klöter, and D. Meschede*
Institut für Angewandte Physik, Universität Bonn, Wegelerstraße 8, 53115 Bonn, Germany

T. Varzhapetyan and D. Sarkisyan
Institute for Physical Research, Armenian Academy of Science, Ashtarak-2, 378410, Armenia
(Received 1 April 2004; revised manuscript received 21 May 2004; published 24 September 2004; publisher error corrected 29 September 2004)

We present saturation and polarization laser spectroscopy experiments of indium vapor with a single color on the 410 nm transition and with two colors at 410 and 451 nm. The spectra observed by polarization spectroscopy are discussed in terms of a quantitative model. The line shapes observed with two-color spectroscopy can phenomenologically be described taking into account hyperfine changing collisions, velocity changing collisions, and dark resonances. As an application, we actively stabilized a 410 nm diode laser on the resonances of saturation and polarization spectroscopy, and obtained long term frequency stabilities in the 100 kHz–1 MHz range.

DOI: 10.1103/PhysRevA.70.033810 PACS number(s): 42.62.Fi, 32.30.Jc, 32.70.Jz, 42.55.Px

I. INTRODUCTION

Laser saturation spectroscopy (see, e.g., [1,2]) and polarization spectroscopy (see, e.g., [2,3]) are methods that allow the generation of sub-Doppler resonances in an atomic vapor. Such signals are important for laser frequency stabilization at the MHz level if spectrally narrow and stable laser light is required.

In this paper we are concerned with high resolution spectroscopy of indium vapor stored in an all-sapphire cell (ASC). It can withstand a temperature of more than 600 °C in order to provide a reasonable atomic density of about 10^{10} cm^{-3} [4]. The goal is to apply this tool for frequency stabilization of lasers at 410 and 451 nm corresponding to the $5P_{1/2} \rightarrow 6S_{1/2}$ and the $5P_{3/2} \rightarrow 6S_{1/2}$ transitions, respectively, see Fig. 1. Because of the technological importance of indium, laser cooling of an In atomic beam [5] could be of interest, for instance, in order to apply the methods of atomic nanofabrication [6]. Since the branching ratio for the decay from the $6S_{1/2}$ state to the $5P_{1/2,3/2}$ ground states is 2:3, the violet (410 nm) and the blue (451 nm) light have to be applied simultaneously for laser cooling because a closed level scheme allowing multiple photon scattering is necessary [5].

II. SATURATION SPECTROSCOPY

For saturation spectroscopy of the $5P_{1/2} \rightarrow 6S_{1/2}$ transition we use 410 nm light generated by an extended cavity diode laser (TOPTICA DL100) with an output power of 15 mW. A standard setup (cf. [2]) is used where an amplitude modulated pump beam ($S_{\mathrm{pump}}=0.7$) counterpropagates the probe beam ($S_{\mathrm{probe}}=0.3$). Here S denotes the saturation parameter defined as $S=I/I_{\mathrm{Sat}}^{\lambda}$, with $I_{\mathrm{Sat}}^{\lambda} \equiv \pi hc\gamma_{\lambda}/(3\lambda^3)$, $I_{\mathrm{Sat}}^{410}=16.9\mathrm{mW/cm}^2$, and $\gamma_{410}=2\pi$ 8.9 MHz [8]. Figure 2 shows the pure and the demodulated transmission signal which in stark contrast to spectra obtained from a commercial hollow cathode lamp exhibits excellent Doppler-free resonances. The observed linewidth of the latter, $\Delta\nu_{\mathrm{FWHM}}=50$MHz, is larger than the natural linewidth of $\gamma_{\mathrm{decay}} \equiv \gamma_{410}+\gamma_{451}=2\pi 25.1$ MHz because of power broadening, a spectral laser linewidth of 10 MHz, a nonperfect alignment of the counterpropagating pump and probe beams, and residual pressure broadening.

III. POLARIZATION SPECTROSCOPY

An alternative technique to obtain narrow sub-Doppler spectra is polarization spectroscopy that has extensively been discussed in the literature (see, e.g., [3,2]). The setup used for the measurements discussed in this paper is sketched in Fig. 3. The 410 nm light is again generated by a diode laser.

The laser beam is split into a pump and a probe beam. The first one is circularly polarized whereas the latter remains linearly polarized. The rotation of the probe beam polarization is analyzed with a polarizing beam splitter (PBS) oriented at an angle of 45° with respect to the initial linear polarization of the probe beam. The difference signal of the two photodiodes PD1 and PD2 measuring the intensities at

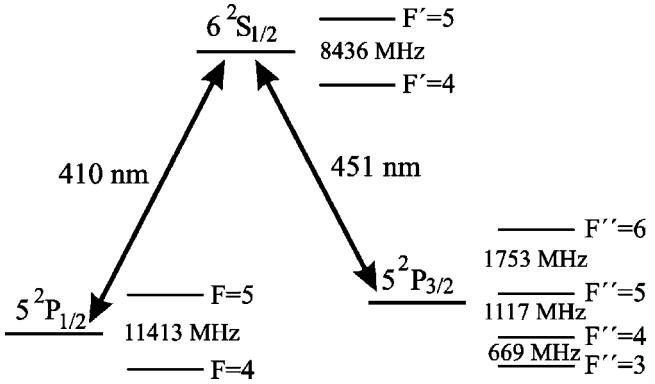

FIG. 1. Energy level scheme of ^{115}In according to [7].

*Electronic address: meschede@iap.uni-bonn.de; URL: http://www.iap.uni-bonn.de/ag_meschede/english/index_eng.html

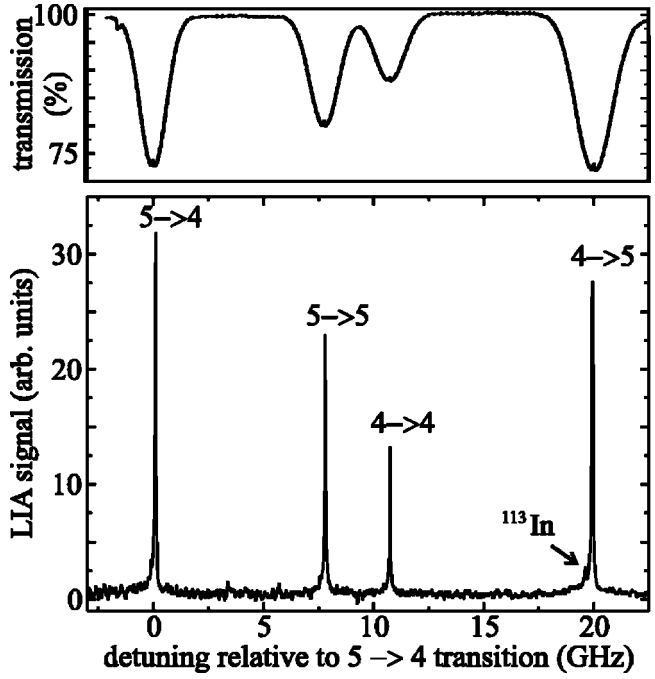

FIG. 2. The transmission signal at 410 nm for saturation spectroscopy with an ASC and a typical pump beam power of about 35 μW (upper graph) and the corresponding demodulated signal (lower graph).

the two ports of the PBS is sensitive to rotations of the probe beam polarization. The resulting spectrum is shown in Fig. 4. For the analysis of this spectrum we write the total rotation Φ_{total} as a sum of the following three main contributions:

(1) light induced circular birefringence (Φ_{CB});

(2) light induced linear dichroism (Φ_{NLFE}); and

(3) magnetic field induced circular birefringence (Φ_{LFE}).

The influence of these contributions can be expressed by the complex index of refraction $n_q \equiv n_r^q + i n_q''$ which is given by

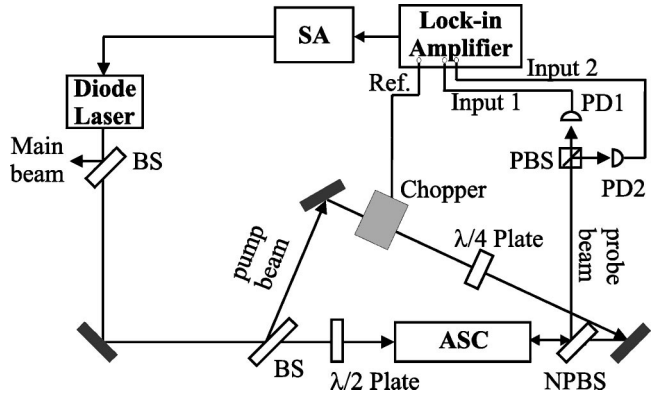

FIG. 3. Setup for polarization spectroscopy. PD1 and PD2: photodiodes measuring the intensities of the two outputs of the polarizing beam splitter (PBS) being oriented at 45° with respect to the linear polarization of the probe beam; BS: beamsplitter; NPBS: nonpolarizing beamsplitter cube; ASC: all-sapphire cell; and SA: servoamplifier.

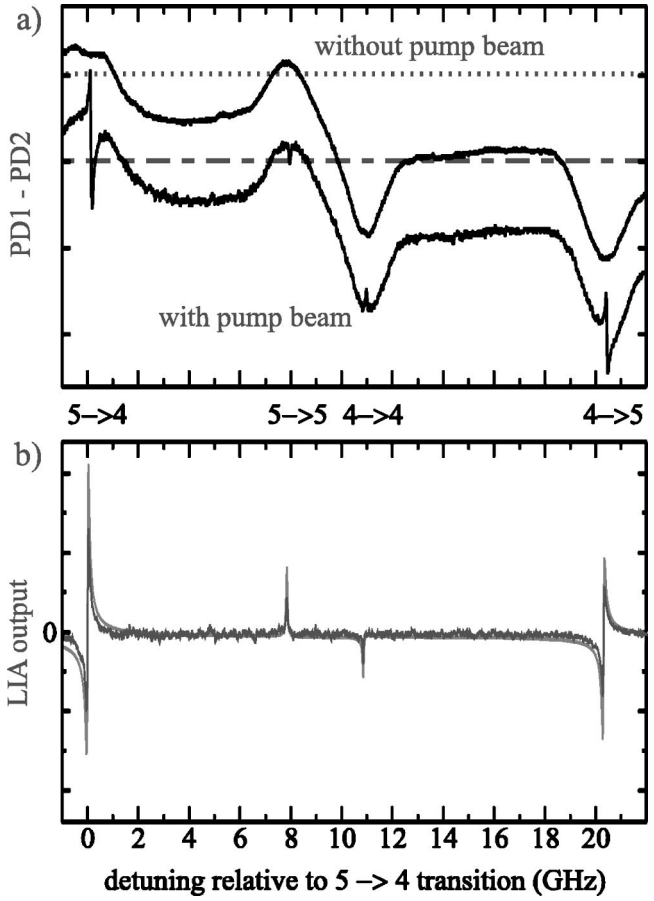

FIG. 4. (a) Difference signal of the two photodiodes PD1 and PD2 with and without a pump beam shone in; the corresponding zero-levels are indicated by the dashed and dotted line, respectively. Both curves show the background due to Φ_{LFE}. (b) Difference of the two curves in (a) obtained by amplitude modulation of the pump beam with a chopper and demodulation with a lock-in amplifier (LIA). The fit takes into account Φ_{CB} as well as Φ_{NLFE}.

$$n_q - 1 = \frac{1}{2\hbar\varepsilon_0} \sum_{m_g} \rho_{m_g} \frac{|\langle F_e, m_g + q | d_q | F_g, m_g \rangle|^2}{(\omega_0 - \omega) - i\gamma_{eg}}. \qquad (1)$$

Here d_q are the tensorial components [$q = \pm 1$ for right (RCP) and left (LCP) circularly polarized light and $q = 0$ for light polarized along the axis of quantization] of the electric dipole operator $\vec{d} \equiv e \cdot \vec{r}$, ρ_{m_g} is the population of the ground state $|F_g, m_g\rangle$, $\langle F_e, m_g + q | d_q | F_g, m_g \rangle$ is the transition matrix element, ω_0 is the resonance frequency, γ_{eg} is the transverse relaxation rate, and ε_0 is the permittivity of vacuum.

A. Light induced circular birefringence

The proper signal of polarization spectroscopy originates from optical pumping inducing a circular birefringence. The linear polarization of the probe beam can be written as a superposition of RCP and LCP light. The two circularly polarized components acquire different phases φ_+ and φ_- when the light traverses the atomic sample with length L. The phase $\varphi_\pm = (n_\pm - 1)kL$ depends on the wave vector $k \equiv 2\pi/\lambda$ of the light with wavelength λ and the complex index of

refraction for RCP and LCP light $n_{\pm}$. By means of the Jones formalism (see, e.g., [9]) the difference signal of PD1 and PD2 measuring the intensities at the two ports of the PBS (see Fig. 3) can, for an optically thin medium, easily be calculated to be

$$\mathcal{S}^{45°+\theta} = I_0 e^{-(n''_- + n''_+)kL} \sin[(n'_- - n'_+)kL - 2\theta] \approx I_0[(n'_- - n'_+)kL - 2\theta] \propto \Phi_{\mathrm{CB}} - 2\theta. \quad (2)$$

The initial intensity of the light is I_0, and $\theta \ll 1$ takes into account nonperfect alignment of the PBS with respect to the horizontal axis. The contributions of the birefringence of the windows can be neglected because the c axis of the sapphire windows is normal to their surface. The expression $(n'_+ - n'_-)kL$ for the circular birefringence in Eq. (2) can be further simplified by using Eq. (1) together with the Wigner-Eckart theorem:

$$n'_- - n'_+ = \frac{|\langle F_e \| d \| F_g \rangle|^2}{2\hbar\varepsilon_0} \mathcal{K}_{ge}^{\mathrm{CB}} \left(\sum_{m_g} \rho_{m_g m_g} \right) \frac{x_\delta}{1 + x_\delta^2} = \frac{|\langle F_e \| d \| F_g \rangle|^2}{2\hbar\varepsilon_0} \mathcal{K}_{ge}^{\mathrm{CB}} \mathcal{P}_z \frac{x_\delta}{1 + x_\delta^2}. \quad (3)$$

This is a dispersive Lorentzian with a line shape determined by the normalized detuning $x_\delta = (\omega - \omega_0)/\gamma_{eg}$ and an amplitude depending on the longitudinal component of the spin polarization $\mathcal{P}_z$, also called orientation, and the factors $\mathcal{K}_{ge}^{\mathrm{CB}}$ which are calculated to be

$$\frac{1}{\mathcal{K}_{ge}^{\mathrm{CB}}} = \begin{cases} -F_g(2F_g+1), & \text{if } F_e = F_g - 1 \\ -F_g(F_g+1)(2F_g+1), & \text{if } F_e = F_g \\ (F_g+1)(2F_g+1), & \text{if } F_e = F_g + 1 \end{cases}.$$

Equations (2) and (3) do not take into account any magnetic field effect.

B. Light induced linear dichroism

If the polarization of the pump beam is not perfectly circular but an ellipse, the chiral symmetry along the propagation axis of the light field is broken. As a consequence, an alignment with the expectation value

$$\mathcal{A}_{zz} = \sum_{m_g} \rho^g_{m_g m_g} [F_g(F_g+1) - 3m_g^2] \quad (4)$$

is induced along the principle axis of the polarization ellipse and acts as an optical axis of birefringence. It has been shown in [10] that the nonlinear Faraday effect (NLFE), which describes this light induced linear birefringence, rotates the linear polarization of light traversing an atomic sample having an alignment by an amount

$$\Phi_{\mathrm{NLFE}} = \frac{1}{2}(n''_{\parallel} - n''_{\perp})kL \frac{y_{\mathrm{B}}}{1 + y_{\mathrm{B}}^2}. \quad (5)$$

Equation (5) describes the dispersive B-field dependence of the NLFE. Here $y_{\mathrm{B}} \equiv 2g_{\mathrm{g}}\omega_{\mathrm{L}}/\gamma_R$ gives the Larmor frequency $\omega_{\mathrm{L}} = \mu_{\mathrm{Bohr}} B/\hbar$ in terms of a ground state relaxation rate γ_R, g_{g} is the g factor of the ground state F_g, and μ_{Bohr} is the Bohr magneton.

The difference of the imaginary parts of the index of refraction for a light field with polarization parallel or perpendicular to the principal axis of the alignment is given by

$$n''_{\parallel} - n''_{\perp} = \frac{|\langle F_e \| d \| F_g \rangle|^2}{2\hbar\varepsilon_0} \mathcal{K}_{ge}^{\mathrm{LD}} \mathcal{A}_{zz} \frac{1}{1 + x_\delta^2}, \quad (6)$$

with the coefficients $\mathcal{K}_{ge}^{\mathrm{LD}}$ that have been calculated in [10] being

$$\frac{1}{\mathcal{K}_{ge}^{\mathrm{LD}}} = \begin{cases} F_g(2F_g-1)(2F_g+1), & \text{if } F_e = F_g - 1 \\ -F_g(F_g+1)(2F_g+1), & \text{if } F_e = F_g \\ (F_g+1)(2F_g+1)(2F_g+3), & \text{if } F_e = F_g + 1 \end{cases}.$$

According to Eq. (6), the NLFE has an absorptive laser frequency dependence. The contribution of the NLFE to the signal $\mathcal{S}^{45°+\theta}$ of Eq. (2) can hence be written as

$$\Phi_{\mathrm{NLFE}} \propto g_{\mathrm{g}} \mathcal{A}_{zz} B \frac{1}{1 + x_\delta^2}. \quad (7)$$

Although the NLFE can only be observed for a nonzero magnetic field, the influence of B on the frequency dependence of the NLFE is not taken into account for our simple model at this point.

Since the expressions given by Eqs. (3) and (4) describing orientation and alignment depend on the populations ρ_{m_g} of the Zeeman sublevels of the six F states in the $5P_{1/2}$ and the $5P_{3/2}$ ground states, the relative contributions of orientation and alignment can be calculated with a rate equation model taking into account all 60 m_F sublevels. For the comparison of the relative peak heights the reduced matrix element $\langle F_e \| d \| F_g \rangle$ must be written in terms of $\langle L_e \| d \| L_g \rangle = \langle S \| d \| P \rangle$ and appropriate $3j$ and $6j$ symbols.

C. Magnetic field induced circular birefringence

The Doppler-broadened structures of the spectrum in Fig. 4(a) adjacent to the signal Eq. (2) have contributions from light self-induced circular and linear birefringence because the probe beam is slightly elliptically polarized. In this case a convolution of Eqs. (3) and (6) and with the atomic velocity distribution (Voigt convolution) is necessary yielding broad dispersive and absorptive line shapes. Since this effect is self-induced it does not depend on the pump beam.

The main contribution to the broad structures is the linear Faraday effect (LFE) which is a magnetic field induced circular birefringence rotating the linear polarization of the probe beam by an amount of (see [11,12])

$$\Phi_{\mathrm{LFE}} = \frac{1}{2}(\tilde{n}'_- - \tilde{n}'_+)kL. \quad (8)$$

This expression is similar to the one obtained in Eq. (2) with the exception that $\tilde{n}'_{\pm}$ have Doppler broadened line shapes and resonance frequencies that are shifted by the Larmor frequency ω_{L} leading to $\omega_{\pm} = \omega_0 + (\Delta g m_g \pm g_e)\omega_{\mathrm{L}}$; here $\Delta g \equiv g_{\mathrm{e}} - g_{\mathrm{g}}$ is the difference of the g factors of the excited (F_e) and ground state (F_g). This together with the wave function mixing described in [11,12] allowed us to calculate the expected spectrum for the frequency dependence of the LFE

with the simulation program used in [12] and showed a qualitatively good agreement with the experimental result.

D. Discussion of the polarization spectrum

At zero magnetic field $\Phi_{total}=\Phi_{CB}$ because Φ_{NLFE} and Φ_{LFE} vanish; the resonance lines have hence a sub-Doppler width. At nonzero magnetic field, also Φ_{NLFE} and Φ_{LFE} contribute to the signal if longitudinal *B*-field components are present [see Fig. 4(a)]. Since Φ_{LFE} does not originate from optical pumping, this background can be removed by amplitude modulating the pump beam with a chopper and demodulating the difference of the signals from photodiodes PD1 and PD2 as described above with a lock-in amplifier. The remaining signal which is due to Φ_{CB} and Φ_{NLFE} is shown in Fig. 4(b).

In order to verify our interpretation of the spectrum in Fig. 4(b) we measured the Stokes parameters of the initially circularly polarized pump beam having traversed the nonpolarizing beam splitter cube (NPBS): the degree of linear and circular polarization yields 0.56 and 0.76, respectively; the polarization ellipse is inclined by an angle of about 20° (25°) with respect to the horizontal plane (the original polarization of the pump beam). Furthermore, we applied additional magnetic fields to the existing stray fields in the ASC and observed that, depending on the strength and the orientation of the magnetic field, Φ_{NLFE} (Φ_{CB}) dominates the signal leading to an absorptive (dispersive) line shape.

Figure 4(b) confirms the prediction of Eq. (7): the peaks for the $5\rightarrow5$ and $4\rightarrow4$ transitions have opposite signs because $g(F_g=4)=-1/15$ and $g(F_g=5)=+1/15$. The relative intensities for Φ_{CB} and Φ_{NLFE} could be determined with a least-squares fit of the experimental spectrum in Fig. 4(b) to be 100:2:5:63 and 100:126:71:43 for the $5\rightarrow4$, $5\rightarrow5$, $4\rightarrow4$, and $4\rightarrow5$ transitions, respectively. The ratios calculated with the rate equation model are 100:5:3:31 and 100:117:64:22 for a pump power of 66 μW ($S_{pump}\approx0.5$) which was used for the measurement of the spectra in Fig. 4. The deviations of the theoretical and the experimental results are probably due to the relatively strong probe beam ($S_{probe}=0.45$) and the nonperfect Gaussian intensity distribution in the laser beams. Furthermore, the theoretical dependence of Φ_{CB} and Φ_{NLFE} on the number of pump cycles is very sensitive.

The deviation also indicates that relaxation processes other than the spontaneous decay and the time of flight within the probe laser beam limit the number of possible pump cycles for a given intensity. We find indeed evidence of strong hyperfine changing collisions, e.g., in two color spectroscopy (see Sec. IV).

It is straightforward to derive an error signal from the polarization spectrum shown in Fig. 4(b) for locking the laser frequency with a servoamplifier in a feedback-loop with a bandwidth of a few 100 Hz. We have characterized the stability of the laser system by analyzing this error signal in terms of Allan variances [13]. A typical result is shown in Fig. 5 for the unlocked laser and the laser locked on the center of the dispersive peak of the $4\rightarrow5$ transition shown in Fig. 4(b). A stability of about 140–200 kHz is achieved for integration times of 1–10 s. The laser remains locked for more than 1 h. This performance, which has also been obtained for saturation spectroscopy, is sufficient for laser cooling applications.

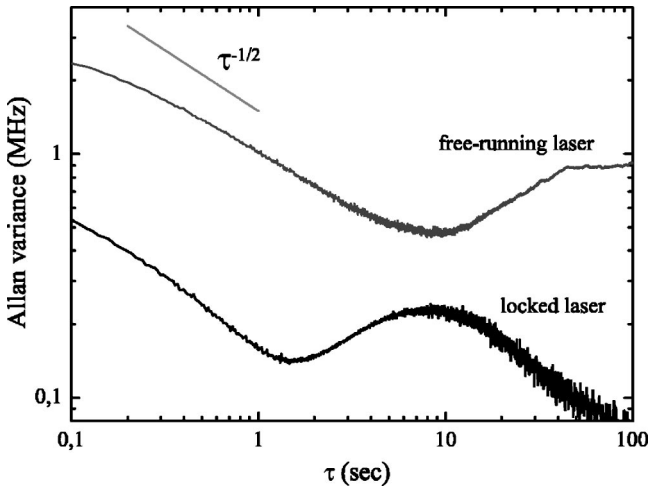

FIG. 5. Allan variance of the error signal for a free-running laser and for the same laser locked on resonance of the $4\rightarrow5$ transition with polarization spectroscopy. The slope for a pure white noise ($\tau^{-1/2}$) is sketched to guide the eye. The total data acquisition time was 70 min.

IV. TWO COLOR SPECTROSCOPY

The blue light at 451 nm is generated by frequency doubling a Ti:Sa laser (MBR E-110). Active frequency stabilization of this light using spectroscopic signals derived from the indium ASC is not straightforward because the signals obtained from the thermal population of the $5P_{3/2}$ state at 630 °C are relatively small; we have measured 6% maximum absorption with a Doppler width of 1.5 GHz.

Optical pumping with the violet laser beam ($S_{410}=0.7$) increases the absorption of the copropagating 451 nm light ($S_{451}=0.2$) having the same diameter of 1 mm from a few percent to more than 10%. While the amplitude modulated violet laser is always locked to the $4\rightarrow5$ transition, we have recorded background-free transmission spectra of the blue laser scanned across the $(5,4,3)\rightarrow4$ transitions [see Fig. 6(a)] and $(6,5,4)\rightarrow5$ transitions [Fig. 6(b)] by demodulating the photocurrent signal with a lock-in amplifier; the photodiode is equipped with an interference filter blocking the 410 nm light. The polarizations of these two laser beams were orthogonal.

The main observations can be summarized as follows.

(1) In all spectra the hyperfine components of the $5P_{3/2}\rightarrow6S_{1/2}$ transition are resolved.

(2) The individual lines show unexpectedly broad peaks with a full width at half maximum (FWHM) of order several hundreds of MHz which is in between the natural linewidth (25 MHz) and the Doppler width (1.5 GHz). Power broadening is negligible.

(3) The line shapes are neither Lorentzian nor Gaussian.

(4) When the violet and the blue laser excite the same

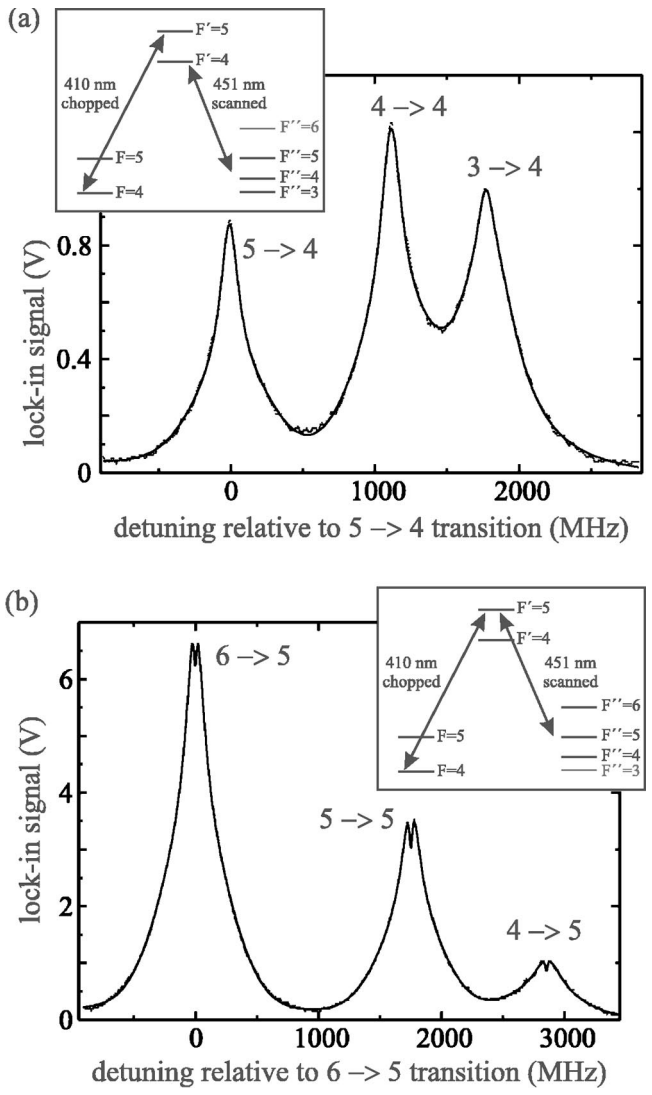

FIG. 6. Lock-in signal and least-squares fit for the transmission of the 451 nm light scanned across the $(5,4,3)\rightarrow 4$ (a) and the the $(6,5,4)\rightarrow 5$ (b) transitions. The amplitude modulated violet laser drives the $4\rightarrow 5$ transition.

upper level ($|6S_{1/2},F'=5\rangle$) the peaks show a narrow dip at their center [Fig. 6(b)] which is not present if different upper levels are excited [Fig. 6(a)].

(5) By varying the violet laser frequency across the Doppler profile of the 410 nm transition the peaks for the 451 nm transition are shifted accordingly while the line shape—including the dip—is not significantly changed; only the amplitude of the peak changes, reflecting the thermal velocity distribution of atoms in the $P_{1/2}$ state.

A detailed theory is beyond the scope of the present paper. Thus we restrict our discussion here to a phenomenological interpretation of our most prominent observations by considering two different kinds of two-photon processes. For both cases discussed below, the violet laser excites atoms from the $|5P_{1/2},F=4\rangle$ level to the $|6S_{1/2},F'=5\rangle$ state from where they spontaneously decay with 60% probability to the $|5P_{3/2},F''=6,5,4\rangle$ levels by dipole transitions. A single velocity class defined by the fixed frequency violet laser should be populated in this process where recoil effects are negligible.

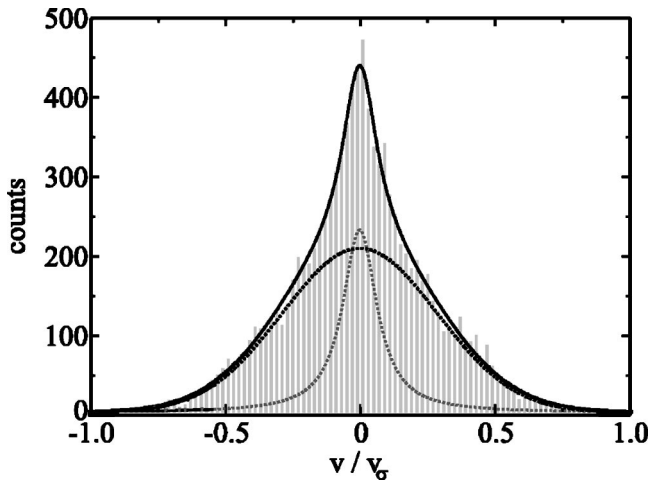

FIG. 7. Simulated velocity distribution of 10 000 atoms initially at rest having undergone one collision with thermal atoms of rms-velocity v_σ. The least-squares fit of this velocity distribution together with the Lorentzian and the Gaussian contribution are also drawn.

A. Stepwise two-photon processes

The spectrum of the $|5P_{3/2},F''=5,4,3\rangle\rightarrow|6S_{1/2},F'=4\rangle$ transitions in Fig. 6(a) shows three lines with a width of order several hundred MHz, where the signal from the $3\rightarrow 4$ transition is observed even though the $F''=3$ level cannot be populated by dipole transitions from the $F'=5$ state.

Phenomenologically we find that we can well approximate the observed profiles of the resonance lines corresponding to the $F''=4,5$ states in Fig. 6(a) with a combination of a Lorentzian and a Gaussian profile with typical FWHM of about 170 and 600 MHz, respectively. Both linewidths by far exceed the breadth expected for a narrow velocity class probed in linear absorption spectroscopy at the level of 30–50 MHz. We attribute the enhanced linewidth to the influence of velocity changing collisions which have been intensely studied for atoms and (typically inert) perturbers at pressures of several hundred to 1000 mTorr (see [14,15]).

While it is impossible here to extract details of the collisional interaction, In-In ground state collisions, light induced collisions [16], and residual gas collisions should be considered. In order to illustrate this interpretation we have carried out a numerical simulation where an initial $v=0$ velocity group is redistributed by a single collision with thermal atoms with the rms-velocity v_σ of identical mass in a hard sphere model. The result of this simple model is a velocity distribution which is also well represented by a combination of a narrow Lorentzian and a wider Gaussian. The width of the Gaussian contribution is about 41% of the width of the initial thermal distribution (see Fig. 7). In our experiment where multiple collisions as well as transit time effects also influence the observed line shape we find similar values.

In our fits the resonance line for $F''=3$ which cannot directly be populated by radiative decay shows a line shape deviating significantly from the other two lines. The fit of the

$3 \rightarrow 4$ resonance line yields a narrow Gaussian and a wider Lorentzian with FWHM of about 460 MHz and 95 MHz, respectively. We attribute this deviation from the lines originating in the $F''=4,5$ states to the fact that the $F''=3$ state is itself populated by collisions. The lines of the spectrum in Fig. 6(b) having the same upper hyperfine level as the violet pump laser can also be analyzed in terms of the phenomenological line-shape model introduced here to describe stepwise processes. The agreement is very good for all lines if one takes also into account the central dip which we attribute to coherent two-photon processes.

B. Coherent two-photon processes

It is well known that Λ-type three level systems can lead to coherent population trapping or electromagnetically induced transparency [17,18]. The dip observed for all spectral lines of Fig. 6(b) corresponds to enhanced transmission of the 451nm laser light and hence reflects such coherent two-photon processes as indicated by its exclusive presence if the two lasers are coupled to the same upper level. The dip can be well approximated by an inverted Lorentzian with a typical width of order 30 MHz.

Coherent two-photon transitions for copropagating laser beams are subject to Doppler broadening with a width of $|k_{410}-k_{451}|\Delta v$ if one frequency is fixed. In our case, Δv is the width of the velocity distribution of the atoms optically pumped with 410 nm light in the $P_{3/2}$ state which corresponds to atoms initially in the $v=0$ class. We thus expect 9.5% of the FWHM of the peak shown in Fig. 8 which is 30 MHz. This is in good agreement with our observation. In Fig. 8 the $5 \rightarrow 4$ transition is directly compared with the $6 \rightarrow 5$ transition of the 451 nm line; the corresponding components of the fit are explicitly shown.

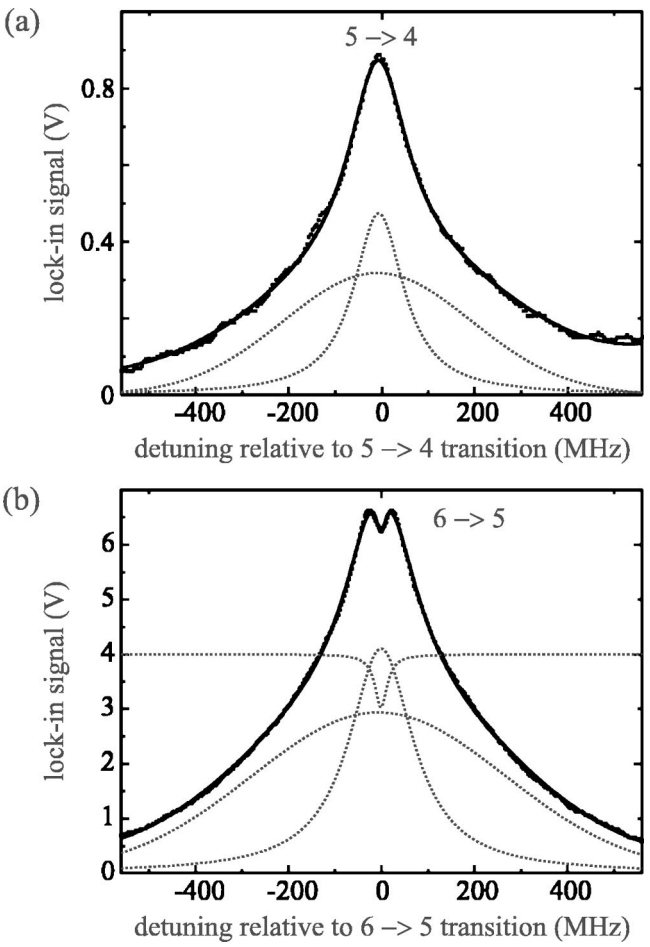

FIG. 8. Experimental data with least-squares fit and the two/three (a)/(b) components of the fit. The narrow Lorentzian in (b) is manually shifted up for reasons of clarity. Note that the signal in (a) is by a factor of 5 smaller than the one in (b).

V. CONCLUSIONS

Standard methods of saturation and polarization spectroscopy can be applied to indium vapor stored in an all-sapphire spectroscopy cell at about 600 °C. Our main conclusion is that saturation spectroscopy works conveniently for all hyperfine transitions of the 410 nm line. Conventional polarization spectroscopy can be used for stabilization purposes for the $F \rightarrow F \pm 1$ transitions with favorable results. On the $F \rightarrow F$ transitions the signal is strongly suppressed while residual magnetic fields generate small absorptive resonances caused by the nonlinear Faraday effect. All spectral lines can be used for laser frequency stabilization.

Two color spectroscopy has revealed unexpected line shapes and linewidths which we attribute to stepwise and coherent two-photon processes; the general line shape can be interpreted in terms of collisional effects. This type of spectroscopy can be used for frequency stabilization of the 451 nm light source if optical pumping with 410 nm creates a nonthermal population of the $5P_{3/2}$ levels. If the violet and the blue light excite the same upper hyperfine level, even a narrow dip appears which can be used to lock the 451 nm light source near the resonance.

ACKNOWLEDGMENTS

The authors acknowledge the contributions by D. Haubrich to this work. Furthermore, we thank P. Berman for the fruitful discussions about velocity changing collisions and H. Metcalf for reading the manuscript. This work was supported by the Deutsche Forschungsgemeinschaft and the European Community within the NANOCOLD IST-2001-32264 project.

[1] O. Schmidt, K.-M. Knaak, R. Wynands, and D. Meschede, Appl. Phys. B: Lasers Opt. **59**, 167 (1994).
[2] W. Demtröder, *Laser Spectroscopy. Basic Concepts and Instrumentation.*, 3rd ed. (Springer-Verlag, Berlin, 2002).
[3] C. Wieman and T. W. Hänsch, Phys. Rev. Lett. **36**, 1170 (1976).
[4] A. N. Nesmeyanov, *Vapor Pressure of the Chemical Elements* (Elsevier, New York, 1963).
[5] H. J. Metcalf and P. van der Straten, *Laser Cooling and Trapping* (Springer, New York, 1999).
[6] D. Meschede and H. Metcalf, J. Phys. D **36**, R17 (2003).
[7] G. V. Deverall, K. W. Meissner, and G. J. Zissis, Phys. Rev. **91**, 297 (1953).
[8] NIST atomic spectra database: http://www.physics.nist.gov/cgi-bin/AtData/main_asd
[9] A. Yariv and P. Yeh, *Optical Waves in Crystals: Propagation and Control of Laser Radiation* (Wiley, New York 1984).
[10] A. Weis, J. Wurster, and S. I. Kanorsky, J. Opt. Soc. Am. B **10**, 716 (1993).
[11] X. Chen, V. L. Telegdi, and A. Weis, J. Phys. B **20**, 5653 (1987).
[12] U. Rasbach, C. Ospelkaus, and A. Weis, Proc. SPIE **4749**, 121 (2002).
[13] D. W. Allan, Proc. IEEE **54**, 221 (1966).
[14] P. R. Berman, Adv. At. Mol. Phys. **13**, 57 (1977), and references therein.
[15] C. Brechignac, R. Vetter, and P. R. Berman, Phys. Rev. A **17**, 1609 (1978).
[16] A. Gallagher and D. E. Pritchard, Phys. Rev. Lett. **63**(9), 957 (1989).
[17] E. Arimondo and G. Orriols, Lett. Nuovo Cimento Soc. Ital. Fis. **17**, 333 (1976).
[18] See, S. E. Harris, Phys. Today **50**(7), 36 (1997), and references therein.